Equivalence relations and symmetries for laboratory, LIDAR, and planetary Müeller matrix scattering geometries

Adrian J. Brown

SETI Institute, 189 N. Bernardo Ave., Mountain View, California 94043, USA (abrown@seti.org)

Received September 3, 2014; revised October 30, 2014; accepted October 31, 2014;
posted November 4, 2014 (Doc. ID 220932); published November 24, 2014

Symmetry relationships for optical observations of matter generally fall into several common scattering geometries. The "planetary" configuration is preferred by observers of extraterrestrial planets, "laboratory" observations are performed in the biomedical research field, and the LIDAR configuration is preferred by those using lasers to probe optical properties of horizontal surfaces with mirror or axial symmetry. This paper begins with the Stokes matrix formalism and uses symmetries of Müller matrix scattering to establish links among the mathematical symmetries of each geometric configuration. We finish the paper by identifying and correcting an influential misapplication of rotational scattering matrices in the literature. The corrected equation should find wide application in models of the LIDAR scattering process.

OCIS codes: (280.3640) Lidar; (290.5870) Scattering, Rayleigh; (010.1615) Clouds; (080.6755) Systems with special symmetry; (290.5855) Scattering, polarization; (010.5620) Radiative transfer.
http://dx.doi.org/10.1364/JOSAA.31.002789

1. INTRODUCTION

Symmetry relationships are key to bringing insight and understanding to complicated physical experiments [1,2]. A survey of modern polarization research literature quickly highlights that Müller matrix polarization observations and experiments fall into two categories. One category is the "planetary" observers, who have been focused on observations of atmospheres around planetary bodies such as Venus or Jupiter [3–5]. On the other hand, the observational setup for "laboratory" (usually in the context of biomedical research [6–8]) or LIDAR observations [9–11] generally fall into another group. Although each group is peripherally aware of the other's work, there is as yet only limited cross comparison of results possible because of the different geometrical reference frames. A recent publication emphasized the need to establish links among these groups [12].

Since most observational situations correspond to either (1) laboratory–bistatic (source and detector widely separated) or (2) planetary–collinear (source and detector parallel and aligned) polarization measurements, most polarization experiments will fall naturally into either of these two configurations. In this paper, the symmetries resulting from these configurations are established explicitly to further our understanding of backscattered electromagnetic radiation.

2. THEORY

We begin with using the Stokes vector to describe an electric field, E [13,14] associated with a plane traveling wave with perpendicular and parallel amplitudes $E_\perp$ and $E_\parallel$ written as

$$\begin{aligned} I &= \langle E_\parallel E_\parallel^* \rangle + \langle E_\perp E_\perp^* \rangle, \\ Q &= \langle E_\parallel E_\parallel^* \rangle - \langle E_\perp E_\perp^* \rangle, \\ U &= \langle E_\parallel E_\perp^* \rangle + \langle E_\perp E_\parallel^* \rangle, \\ V &= i(\langle E_\parallel E_\parallel^* \rangle + \langle E_\perp E_\perp^* \rangle), \end{aligned} \tag{1}$$

where angled brackets $\langle\rangle$ indicate a time average and $*$ indicates complex conjugation.

The Müller matrix of an optical system is represented by elements $M_{11} \ldots M_{44}$. A generic optical system may then be represented by the system's Müller matrix M times the input Stokes vector I_0:

$$I = MI_0 = \begin{pmatrix} M_{11} & M_{12} & M_{13} & M_{14} \\ M_{21} & M_{22} & M_{23} & M_{24} \\ M_{31} & M_{32} & M_{33} & M_{34} \\ M_{41} & M_{42} & M_{43} & M_{44} \end{pmatrix} \begin{pmatrix} I_0 \\ Q_0 \\ U_0 \\ V_0 \end{pmatrix}. \tag{2}$$

For any scattering matrix $F(\mu, \theta)$, (temporarily suppressing the μ, θ dependence), the law of reciprocity [15,16] requires that

$$F = \Delta_3 F^T \Delta_3, \tag{3}$$

where T indicates transpose and Δ_3 is defined as

$$\Delta_3 = \begin{pmatrix} 1 & 0 & 0 & 0 \\ 0 & 1 & 0 & 0 \\ 0 & 0 & -1 & 0 \\ 0 & 0 & 0 & 1 \end{pmatrix}. \tag{4}$$

A similar relation exists for media with isotropic mirror symmetry. The mirror symmetry relation implies that

$$F = \Delta_{3,4} F \Delta_{3,4}, \tag{5}$$

where $\Delta_{3,4}$ is defined as

$$\Delta_{3,4} = \begin{pmatrix} 1 & 0 & 0 & 0 \\ 0 & 1 & 0 & 0 \\ 0 & 0 & -1 & 0 \\ 0 & 0 & 0 & -1 \end{pmatrix}. \tag{6}$$

In any target for which the mirror symmetry and law of reciprocity holds, the scattering matrix is reduced to six independent elements [14] as

$$F = \begin{pmatrix} a_1 & b_1 & 0 & 0 \\ b_1 & a_2 & 0 & 0 \\ 0 & 0 & a_3 & b_2 \\ 0 & 0 & -b_2 & a_4 \end{pmatrix}. \tag{7}$$

The rotation matrix, $L(\alpha)$, for an optical system for counterclockwise rotation (looking in the direction of propagation) by an angle is defined as

$$L(\alpha) = \begin{pmatrix} 1 & 0 & 0 & 0 \\ 0 & \cos 2\alpha & \sin 2\alpha & 0 \\ 0 & -\sin 2\alpha & \cos 2\alpha & 0 \\ 0 & 0 & 0 & 1 \end{pmatrix}. \tag{8}$$

A. Planetary Observations

The planetary scattering geometry is represented in Fig 1(a). Typically, this is a bistatic measurement where a large distance separates source and detector. When an observation is made of a planetary surface or atmosphere for off-zenith illumination, two rotations of the plane of reference are required to transform the incident beam into the scattered beam:

$$\begin{aligned} Z_{\text{planet}}(\theta, \sigma_1, \sigma_2) &= L(\pi - \sigma_2) F(\theta) L(-\sigma_1), \\ Z_{\text{planet}}(\theta, \sigma_1, \sigma_2) &= L(-\sigma_2) F(\theta) L(-\sigma_1). \end{aligned} \tag{9}$$

Equation (9) is Eq. (213) from p. 40 of Chandrasekhar [17]. The second relation comes from the periodic characteristics of L. Z is termed the phase matrix [18]. Expanding this equation using Eqs. (7) and (8), we obtain

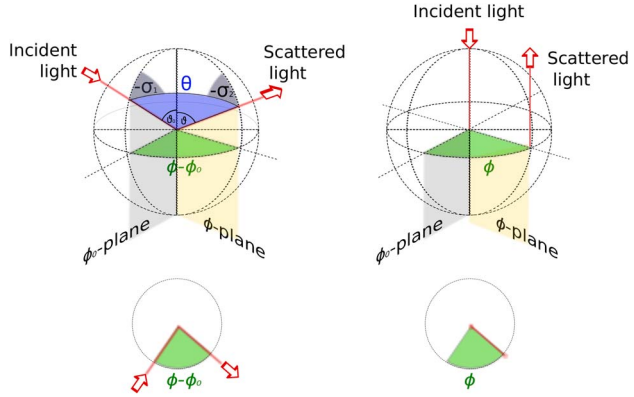

Fig. 1. (a) Planetary observation geometry. (b) Laboratory or LIDAR observation geometry.

$$Z_{\text{planet}}(\theta, \sigma_1, \sigma_2) = \begin{pmatrix} a_1 & b_1 C_1 & -b_1 S_1 & 0 \\ b_1 C_2 & a_2 C_1 C_2 - a_3 S_1 S_2 & -a_2 S_1 C_2 - a_3 C_1 S_2 & -b_2 S_2 \\ b_1 S_2 & a_2 C_1 S_2 + a_3 C_2 S_1 & -a_2 S_1 S_2 + a_3 C_1 C_2 & b_2 C_2 \\ 0 & -b_2 S_1 & -b_2 C_1 & a_4 \end{pmatrix}, \tag{10}$$

where $C_1 = \cos 2\sigma_1$, $C_2 = \cos 2\sigma_2$, $S_1 = \sin 2\sigma_1$, and $S_2 = \sin 2\sigma_2$.

As discussed in Brown and Xie [12], a special geometry exists for observational geometries, where $\sigma_2 = 0$ (observer at zenith, source anywhere). In this case, the following equation,

$$Z_{\text{planet}}(\theta, \sigma_1, 0) = \begin{pmatrix} a_1 & b_1 C_1 & -b_1 S_1 & 0 \\ b_1 & a_2 C_1 & -a_2 S_1 & 0 \\ 0 & a_3 S_1 & a_3 C_1 & b_2 \\ 0 & -b_2 S_1 & -b_2 C_1 & a_4 \end{pmatrix}, \tag{11}$$

holds.

When $\sigma_1 = 0$ (observer anywhere, source at zenith), the following relationship,

$$Z_{\text{planet}}(\theta, 0, \sigma_2) = \begin{pmatrix} a_1 & b_1 & 0 & 0 \\ b_1 C_2 & a_2 C_2 & -a_3 S_2 & -b_2 S_2 \\ b_1 S_2 & a_2 S_2 & a_3 C_2 & b_2 C_2 \\ 0 & 0 & -b_2 & a_4 \end{pmatrix}, \tag{12}$$

holds for the planetary geometry.

B. Laboratory or LIDAR Observations

In a laboratory or LIDAR observation, the source and detector are typically collinear, as seen in Fig. 1(b). When an observation is made in the laboratory or by a LIDAR of a horizontal surface, just two rotations of the observation frame are necessary [19]. However, each rotation is of the same angle (in opposite directions), as

$$\begin{aligned} Z_{\text{lab}}(\theta, \sigma) &= L(\pi - \sigma) F(\theta) L(\sigma), \\ Z_{\text{lab}}(\theta, \sigma) &= L(-\sigma) F(\theta) L(\sigma). \end{aligned} \tag{13}$$

Note that Eq. (13) is similar in theme, but different in detail to those proposed by various previous works [9,10,19–21]. It is most similar to Eq. (13) of [10], although it was not used in the same manner by those authors. As will be further discussed, this formulation is the only one that can match existing experimental results in the literature [7]. Again, the second relation comes from the periodic characteristics of L. Expanding Eq. (13) using Eqs. (7) and (8) or putting $C = C_1 = C_2$ and $S = S_1 = S_2$ in Eq. (10), one obtains

$$Z_{\text{lab}}(\theta, \sigma) = \begin{pmatrix} a_1 & b_1 C & b_1 S & 0 \\ b_1 C & a_2 C^2 + a_3 S^2 & (a_2 - a_3) CS & -b_2 S \\ b_1 S & (a_2 - a_3) CS & a_2 S^2 + a_3 C^2 & b_2 C \\ 0 & b_2 S & -b_2 C & a_4 \end{pmatrix}. \tag{14}$$

As for the planetary observations, special geometries exist in the laboratory situation when $\sigma = 0$. For this case, the following scattering matrix,

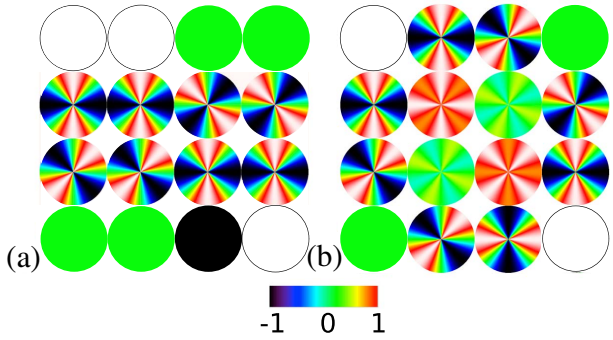

Fig. 2. Rotational symmetries of (a) planetary [Eq. (12)] and (b) laboratory [Eq. (14)] observations. Note that, to match the standard representations of Müller matrix hemispherical maps, the y axis points down in these images. All coefficients except a_3 have been set to 1 to emphasize the rotational dependences. See text for further discussion.

$$Z_{\text{lab}}(\theta,0)=\begin{pmatrix} a_1 & b_1 & 0 & 0 \\ b_1 & a_2 & 0 & 0 \\ 0 & 0 & a_3 & b_2 \\ 0 & 0 & -b_2 & a_4 \end{pmatrix}, \tag{15}$$

holds.

C. Comparisons of Rotational Symmetries of Configurational States

The differences and similarities between the "planetary" and "laboratory/LIDAR" modes are thus summarized in Eqs. (10) and (14). In order to break the degeneracy of Eq. (10), we make a choice to view from the zenith with $\sigma_1=0$, thus obtaining Eq. (12).

The differences in rotational symmetries of the two configurations can be characterized in the following manner. Setting the scattering coefficients a_1, a_2, a_4, b_1, and $b_2=1$ and $a_3=0.5$, we can evaluate the trigonometric dependence on the scattering geometry. Carrying out this substitution in Eqs. (12) and (14), we arrive at the results in Fig. 2.

By comparisons of any Müller matrix hemispherical maps within Fig. 2, we can quickly establish the nature of the geometric configuration used to produce the map. As a useful mnemonic, the laboratory configuration is more "complicated" because there are more constant matrix elements (eight versus four), and the central matrix elements (M_{22}, M_{23}, M_{33}, M_{32}) have twofold rotational symmetry rather than the fourfold rotational symmetry of their planetary counterparts.

D. Equivalence Relations

The equivalence relations for the zenith laboratory [Eq. (12)] and planetary [Eq. (14)] observations can therefore be expressed as

$$\begin{aligned} a_{1\text{planet}} &= a_{1\,\text{lab}}, \\ a_{2\text{planet}} &= \frac{C^2}{C_2}a_{2\,\text{lab}}+\frac{S^2}{C_2}a_{3\,\text{lab}}, \\ a_{3\text{planet}} &= \frac{S^2}{C_2}a_{2\,\text{lab}}+\frac{C^2}{C_2}a_{3\,\text{lab}}, \\ a_{4\text{planet}} &= a_{4\,\text{lab}}, \\ b_{1\,\text{planet}} &= b_{1\,\text{lab}}\cdot\frac{S}{S_1}, \\ b_{2\,\text{planet}} &= b_{2\,\text{lab}}\cdot\frac{S}{S_1}. \end{aligned} \tag{16}$$

All of these relations can be evaluated from experimental measurements of the same scattering target in either frame, and they then may be used to convert to the other scattering geometry.

3. ANALYTICAL EXAMPLE

To test the veracity of the formulation outlined above, we present a simple application of the ideas presented here, using the analytically tractable electric dipole or Rayleigh scattering matrix [22] as an example.

The scattering matrix for a dipole, as discussed by [17] is given by

$$F_{\text{dipole}}(\theta)=\begin{pmatrix} (3/4)(1+\cos^2\theta) & (-3/4)(\sin^2\theta) & 0 & 0 \\ (-3/4)(\sin^2\theta) & (3/4)(1+\cos^2\theta) & 0 & 0 \\ 0 & 0 & (3/2)\cos\theta & 0 \\ 0 & 0 & 0 & (3/2)\cos\theta \end{pmatrix}. \tag{17}$$

When we use this scattering matrix in Eq. (9) for the planetary scattering geometry, we obtain

$$Z_{\substack{\text{planet}\\\text{dipole}}}(\theta,\sigma_1,\sigma_2)=\begin{pmatrix} (3/4)(1+c^2) & (-3/4)C_1s^2 & (3/4)S_1s^2 & 0 \\ (-3/4)C_2s^2 & (3/4)(1+c^2)C_1C_2-(3/2)cS_1S_2 & (-3/4)(1+c^2)S_1C_2-(3/2)cC_1S_2 & 0 \\ (-3/4)S_2s^2 & (3/4)(1+c^2)C_1S_2+(3/2)cS_1C_2 & (-3/4)(1+c^2)S_1S_2+(3/2)cC_1C_2 & 0 \\ 0 & 0 & 0 & (3/2)c \end{pmatrix}, \tag{18}$$

where $c=\cos\theta$, $s=\sin\theta$, $C_1=\cos 2\sigma_1$, $S_1=\sin 2\sigma_1$, and $C_2=\cos 2\sigma_2$, $S_2=\sin 2\sigma_2$.

For the special case where $\sigma_1=0$ (normal incident light), we have

$$Z_{\substack{\text{planet}\\\text{dipole}}}(\theta,0,\sigma_2)=\begin{pmatrix} (3/4)(1+c^2) & (-3/4)s^2 & 0 & 0 \\ (-3/4)C_2s^2 & (3/4)(1+c^2)C_2 & (3/2)cS_2 & 0 \\ (-3/4)S_2s^2 & (3/4)(1+c^2)S_2 & (3/2)cC_2 & 0 \\ 0 & 0 & 0 & (3/2)c \end{pmatrix}. \tag{19}$$

For the laboratory scattering geometry, we substitute Eqs. (8) and (17) into Eq. (13), to get:

$$Z_{\underline{\text{lab}}}_{\text{dipole}}(\theta,\sigma_1,\sigma_2)=\begin{pmatrix}(3/4)(1+c^2) & (-3/4)Cs^2 & (3/4)Ss^2 & 0\\ (-3/4)Cs^2 & (3/4)(1+c^2)C^2-(3/2)cS^2 & (-3/4)(1+c^2)SC-(3/2)cCS & 0\\ (-3/4)Ss^2 & (3/4)(1+c^2)CS+(3/2)cSC & (-3/4)(1+c^2)S^2+(3/2)cC^2 & 0\\ 0 & 0 & 0 & (3/2)c\end{pmatrix}. \tag{20}$$

A comparison of Eqs. (19) and (20) allows us to assess how dipole scattering is manifested in hemispherical scattering for planetary (normal incidence) and laboratory settings, respectively. It can be seen that laboratory standard settings give more complicated terms (compare M_{22}, M_{23}, M_{32}, M_{33}), but the M_{11} term and the last row and column are identical. M_{21} and M_{31} are relatively similar, as is M_{12}; however, M_{13} is zero in the planetary configuration.

Figure 3 displays 16 Müller matrix hemispherical maps for a Rayleigh scattering target produced using the adding–doubling approach. This compares favorably with Eq. (19).

A. Notes on Effects of Mirrors in Beam Path

The Müller matrix for a perfect mirror for light at normal incidence is [23] [Eq. (33.71)]

$$M_R=\begin{pmatrix}1&0&0&0\\0&1&0&0\\0&0&-1&0\\0&0&0&-1\end{pmatrix}. \tag{21}$$

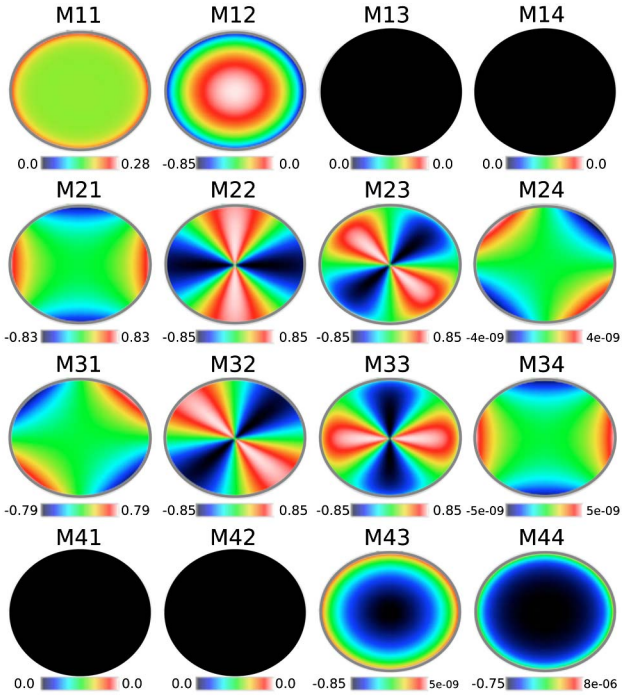

Fig. 3. Müller matrix images of backscattered photons scattered from a Rayleigh scattering particle. The particle is single scattering and is 0.01 μm in diameter. The laser light is $\lambda = 1$ μm. The calculations use a spherical target modeled by an adding–doubling approach. The incident light is normal to the target. Color scales indicate intensity relative to the M11 element. See text for discussion of symmetries.

When the perfect mirror is inclined at angle θ to the incoming beam, the Müller matrix is modified as [e.g., MSE Memo [24] 20c, Eq. (12)]:

$$M_R(\theta)=\begin{pmatrix}1&0&0&0\\0&\cos 4\theta&\sin 4\theta&0\\0&-\sin 4\theta&\cos 4\theta&0\\0&0&0&-1\end{pmatrix} \tag{22}$$

Therefore, when the mirror is inclined 45°, the ideal mirror Müller matrix becomes

$$M_R\left(\frac{\pi}{4}\right)=\begin{pmatrix}1&0&0&0\\0&-1&0&0\\0&0&-1&0\\0&0&0&-1\end{pmatrix}. \tag{23}$$

When we use the mirror matrix in Eq. (22) for the laboratory/LIDAR scattering geometry, the mirror is inclined 90° to the beam, so the mirror Müller matrix becomes

$$M_R\left(\frac{\pi}{2}\right)=\begin{pmatrix}1&0&0&0\\0&1&0&0\\0&0&1&0\\0&0&0&-1\end{pmatrix}. \tag{24}$$

4. DISCUSSION

A. Müller Matrix On–Off Diagonal Symmetries

Feng [20] noted that the results presented by Hielscher *et al.* [6] indicated that all off-diagonal Müller matrix maps for Mie and Rayleigh scattering should obey symmetry rules. Feng stated that M_{12} and M_{21}, M_{32} and M_{23}, and M_{31} and M_{13} should be symmetric, whereas M_{43} and M_{34}, M_{24} and M_{42} should be antisymmetric. He established that, if instead of Eq. (13), one uses $R(\varphi)M'(\theta)R(-\varphi)$ [his Eq. (11)], one obtains these symmetry relationships. He matched this to a range of results in the literature [6,25] and contrasted it with the work of Raković *et al.* [19]. However, Feng did not discuss the relationship between on-diagonal elements M_{22} and M_{33} and their tight linkage to elements M_{23} and M_{32} in the backscattering geometry. When one compares with more recent experimental work [26,27] (not cited by Feng), one realizes that it is necessary to adopt the lab phase matrix equation given here [Eq. (13)] in order to fulfill the requirement that $M_{22} \sim -M_{33}$ and $M_{23} \sim M_{32}$(see Fig. 2 of [27] and Fig. 3 of [26]). The same relationship among M_{22}, M_{33}, M_{23}, and M_{32} is found in Figs. 3 and 4 of [25] and Figs. 5, 6, 8, and 9 of [6] (which were cited by Feng), so this relationship is likely to be reliable. By simply employing (ideal) mirror reflections, as discussed above, one *cannot* obtain this symmetry.

Wang *et al.* [21,28] followed the same modeling approach as Raković *et al.*, and their results have similar weaknesses, as pointed out by Feng [20]. In addition, it should be noted that in Raković *et al.*, the element S_{33} (in Fig. 4 of [19]) is inconsistent with Eq. (30b) of that same paper.

B. Effect of Mirror Reflections

It seems likely that the mirror relations in Eqs. (21)–(24) may explain some differences between previous papers in the literature. For example, applying Eq. (24) on the back and front of Xu's Fig. 3 of [26], one obtains a match for Ramella-Roman *et al.* (Fig. 2 of [27]).

In addition, applying Eq. (23) back and front to Figs. 5, 6, 8, and 9 of Hielscher *et al.* [6] brings them into concordance with the results of Ramella-Roman *et al.* (Fig. 2 of [27]). Unfortunately, according to the Hielscher *et al.* description, his optical setup actually involves two 90° mirrors on either side of the sample, suggesting application of Eq. (24) might be more appropriate. We leave resolution of this question for future work.

We have followed a strategy of trusting the experimental results reported in Ramella-Roman *et al.* [27] because these are the most recent laboratory results from an experienced optical group. However, the mathematical approach in Ramella-Roman was not fully characterized because only simple descriptions of an optical setup were given with no mathematical relationship to govern the effect of the mirrors mentioned (in the text on p. 10394 of [27]). Undoubtedly, the results presented here are not the last word on this matter, but one can hope that the direction of future research is now made somewhat clearer. Nonideal mirrors also may play a role in the final resolution of these relationships. Further experimental work is needed to verify the relations in Eq. (13) in the laboratory with a well-characterized optical configuration, including knowledge of mirror angles and nonideal properties.

C. Applications and Comparisons with Other Recent Müller Matrix Studies

Müller matrix analysis has recently been used for size determination of industrial products [29,30]. Biomedical applications of Müller matrix measurements have sought to use polarimetry to image cancerous cells through tissue [31]. To test and calibrate the data gathered from these biomedical imagers, Monte Carlo schemes are very popular [7,25,32,33]. Hopefully, the results of this paper will be helpful in this area.

D. Anisotropic Scatterers

In an interesting recent study, Alali *et al.* [34] used a Monte Carlo approach to examine the axial heterogenity of birefringent materials using polarized light. They developed an "asymmetry degree (ASD)" in Eqs. (18) and (19) based on six off-diagonal elements of the Müller matrix and tested the ASD metric experimentally on stretched polyamide samples, which provided an anisotropic experimental target. In addition, Zeng *et al.* [35] developed rotation-independent polarization Müller-matrix-based parameters for use in characterization of anisotropic scattering objects, which require a full 16-element Müller matrix because they are anisotropic scatterers. Sun *et al.* [36] then tested their applicability on textile samples.

Ossikovski *et al.* have developed several alternative decompositions of the Müller matrix and have addressed the symmetries of these decompositions [37,38]. In addition, Gil and José have recently presented an algebraic decomposition of Müller matrices [39]. Yurkin [40] approached the polarization measurement problem from several different angles. His approach was to look at integrals over the azimuth in order to simulate the Müller matrix symmetries measured using flow cytometry. All these Müller matrix studies will benefit from the equivalence relations derived in this study.

5. CONCLUSIONS

This paper has outlined theoretical linkages between the scattering Müller matrices for "planetary" and "LIDAR/laboratory" observations. Thus, the scene is now set for further advances linking the fields of planetary and laboratory or field observations. Instrument development [41] to study these linkages should go hand in hand with the theories developed here to investigate aspects such as curve fitting of spectral observations of polarization arising from absorption bands [42], broken symmetries, and intercomparisons of Monte Carlo and adding–doubling methods. The successful application analysis of data for terrestrial and planetary missions (such as recently proposed by [43]) utilizing polarization observations relies on interpretations such as those carried out here.

ACKNOWLEDGMENTS

National Aeronautics and Space Administration (NASA) (NNX11AP23G, NNX13AN21G).

REFERENCES

1. J. H. Conway, H. Burgeil, and C. Goodman-Strauss, *The Symmetries of Things* (A. K. Peeters, 2008).
2. H. Weyl, *Symmetry* (Princeton University, 1983).
3. J. W. Hovenier and J. F. de Haan, "Polarized light in planetary atmospheres for perpendicular directions," Astron. Astrophys. **146**, 185–191 (1985).
4. J. F. De Haan, "Effects of aerosols on the brightness and polarization of cloudless planetary atmospheres," Ph.D. thesis (Free University of Amsterdam, 1987).
5. R. Lawless, Y. Xie, P. Yang, G. W. Katawar, and I. Laszlo, "Polarization and effective Mueller matrix for multiple scattering of light by nonspherical ice crystals," Opt. Express **14**, 6381–6393 (2006).
6. A. Hielscher, A. Eick, J. Mourant, D. Shen, J. Freyer, and I. Bigio, "Diffuse backscattering Mueller matrices of highly scattering media," Opt. Express **1**, 441–453 (1997).
7. J. Ramella-Roman, S. Prahl, and S. Jacques, "Three Monte Carlo programs of polarized light transport into scattering media: part I," Opt. Express **13**, 4420–4438 (2005).
8. B. D. Cameron, Y. Li, and A. Nezhuvingal, "Determination of optical scattering properties in turbid media using Mueller matrix imaging," J. Biomed. Opt. **11**, 054031 (2006).
9. A. Ambirajan and D. C. Look, "A backward Monte Carlo study of the multiple scattering of a polarized laser beam," J. Quant. Spectrosc. Radiat. Transfer **58**, 171–192 (1997).
10. D. W. Mueller and A. L. Crosbie, "Analytical expressions for the radiation emergent from a scattering medium exposed to a polarized laser beam," J. Quant. Spectrosc. Radiat. Transfer **67**, 395–428 (2000).
11. S. R. Pal and A. I. Carswell, "Polarizaton properties of lidar backscattering from clouds," Appl. Opt. **12**, 1530–1535 (1973).
12. A. J. Brown and Y. Xie, "Symmetry relations revealed in Mueller matrix hemispherical maps," J. Quant. Spectrosc. Radiat. Transfer **113**, 644–651 (2012).
13. G. G. Stokes, "On the composition and resolution of streams of polarized light from different sources," Trans. Cambridge Philos. Soc. **9**, 399–416 (1852) [reprinted in *Mathematical and Physical Papers* (Cambridge University, 1901), Vol. III].
14. F. Perrin, "Polarization of light scattered by isotropic opalescent media," J. Chem. Phys. **10**, 415–427 (1942).

15. L. Rayleigh, *The Theory of Sound* (Macmillan, 1877).
16. R. S. Krishnan, "The reciprocity theorem in colloid optics and its generalisation," in *Proceedings of the Indian Academy of Science Section A* (Indian Academy of Sciences, 1938), Vol. **7**, pp. 21–34, 15.
17. S. Chandrasekhar, *Radiative Transfer* (Dover, 1960).
18. J. W. Hovenier, C. V. M. van der Mee, and H. Domke, *Transfer of Polarized Light in Planetary Atmospheres—Basic Concepts and Practical Methods* (Springer, 2004).
19. M. J. Raković, G. W. Kattawar, M. Mehrűbeoğlu, B. D. Cameron, L. V. Wang, S. Rastegar, and G. L. Coté, "Light backscattering polarization patterns from turbid media: theory and experiment," Appl. Opt. **38**, 3399–3408 (1999).
20. Y. Feng, "Revisit to the symmetry relations in diffusely backscattered polarization patterns of turbid media," Chin. Opt. Lett. **4**, 667–670 (2006).
21. X. Wang, G. Yao, and L. V. Wang, "Monte Carlo model and single-scattering approximation of the propagation of polarized light in turbid media containing glucose," Appl. Opt. **41**, 792–801 (2002).
22. A. J. Brown, "Spectral bluing induced by small particles under the Mie and Rayleigh regimes," Icarus **239**, 85–95 (2014).
23. D. Goldstein, *Polarized Light*, 2nd ed. (Marcel Dekker, 2003).
24. S. Scott and H. Yuh, *Motonal Stark Effect Memo Series* (MIT, 2004).
25. S. Bartel and A. H. Hielscher, "Monte Carlo simulations of the diffuse backscattering Mueller matrix for highly scattering media," Appl. Opt. **39**, 1580–1588 (2000).
26. M. Xu, "Electric field Monte Carlo simulation of polarized light propagation in turbid media," Opt. Express **12**, 6530–6539 (2004).
27. J. C. Ramella-Roman, S. A. Prahl, and S. L. Jacques, "Three Monte Carlo programs of polarized light transport into scattering media: part II," Opt. Express **13**, 10392–10405 (2005).
28. X. Wang and L. V. Wang, "Propagation of polarized light in birefringent turbid media: a Monte Carlo study," J. Biomed. Opt. **7**, 279–290 (2002).
29. J. Dillet, C. Baravian, F. Caton, and A. Parker, "Size determination by use of two-dimensional Mueller matrices backscattered by optically thick random media," Appl. Opt. **45**, 4669–4678 (2006).
30. A. Parker, C. Baravian, F. Caton, J. Dillet, and J. Mougel, "Fast optical sizing without dilution," Food Hyd. **21**, 831–837 (2007).
31. N. Ghosh, A. Banerjee, and J. Soni, "Turbid medium polarimetry in biomedical imaging and diagnosis," Eur. Phys. J. Appl. Phys. **54**, 30001 (2011).
32. A. Doronin and I. Meglinski, "Online object oriented Monte Carlo computational tool for the needs of biomedical optics," Biomed. Opt. Express **2**, 2461–2469 (2011).
33. E. Berrocal, D. L. Sedarsky, M. E. Paciaroni, I. V. Meglinski, and M. A. Linne, "Laser light scattering in turbid media Part I: Experimental and simulated results for the spatial intensity distribution," Opt. Express **15**, 10649–10665 (2007).
34. S. Alali, Y. Wang, and I. A. Vitkin, "Detecting axial heterogeneity of birefringence in layered turbid media using polarized light imaging," Biomed. Opt. Express **3**, 3250–3263 (2012).
35. N. Zeng, J. Xiaoyu, G. Qiang, H. Yonghong, and M. Hui, "Linear polarization difference imaging and its potential applications," Appl. Opt. **48**, 734–739 (2009).
36. M. Sun, H. He, N. Zeng, E. Du, Y. Guo, C. Peng, Y. He, and H. Ma, "Probing microstructural information of anisotropic scattering media using rotation-independent polarization parameters," Appl. Opt. **53**, 2949–2955 (2014).
37. R. Ossikovski, A. De Martno, and S. Guyot, "Forward and reverse product decompositions of depolarizing Mueller matrices," Opt. Lett. **32**, 689–691 (2007).
38. R. Ossikovski, "Alternative depolarization criteria for Mueller matrices," J. Opt. Soc. Am. A **27**, 808–814 (2010).
39. J. J. Gil and I. S. José, "Explicit algebraic characterization of Mueller matrices," Opt. Lett. **39**, 4041–4044 (2014).
40. M. A. Yurkin, "Symmetry relations for the Mueller scattering matrix integrated over the azimuthal angle," J. Quant. Spectrosc. Radiat. Transfer **131**, 82–87 (2012).
41. A. J. Brown, B. Suter, and S. Dunagan, "The MARTE imaging spectrometer experiment: design and analysis," Astrobiology **8**, 1001–1011 (2008).
42. A. J. Brown, "Spectral curve fitting for automatic hyperspectral data analysis," IEEE Trans. Geosci. Remote Sens. **44**, 1601–1608 (2006).
43. A. J. Brown, T. I. Michaels, S. Byrne, W. Sun, T. N. Titus, A. Colaprete, M. J. Wolff, G. Videen, and C. J. Grund, "The case for a modern, multiwavelength, polarization-sensitive LIDAR in orbit around Mars," J. Quant. Spectrosc. Radiat. Transfer **132**, doi:10.1016/j.jqsrt.2014.10.021 (to be published).